

## CdS Nanoparticles: A Facile route to Size-Controlled Synthesis of Quantum Dots on a Polymer Matrix

N. Memarian\*

Faculty of Physics, Semnan University, 35131-19111 Semnan, Iran

(Received 21 February 2017; revised manuscript received 04 May 2017; published online 30 June 2017)

An efficient route for fabrication of cadmium sulfide nanoparticles in polymer matrix is presented in this paper. CdS quantum dots have been prepared in polyvinyl alcohol (PVA) by SILAR method. The effect of cycle number on physical properties of CdS nanoparticles has been studied. The optical, structural and morphological properties of nanocrystal samples were characterized by *Uv-Vis* absorbance, X-Ray Diffraction (XRD) and atomic force microscopy (AFM), respectively. The shift of optical absorption edge to shorter wavelengths, than that for the bulk CdS, indicates that the nanometer-sized particles represent the quantum confinement effects. The band gaps are calculated from the optical absorption studies, ranging from 2.88 to 2.41 eV. Particle sizes are estimated from the effective mass approximation. In addition, particle sizes are calculated from the XRD studies that are in good agreement with those estimated from the band gap values. XRD results illustrate nanocrystals have cubic structure with (111) preferred orientation. AFM pictures of the CdS/PVA surfaces show cluster formation of nanoparticles.

**Keywords:** CdS, Nanoparticles, SILAR method, Polymer matrix.

DOI: [10.21272/jnep.9\(3\).03027](https://doi.org/10.21272/jnep.9(3).03027)

PACS numbers: 61.46. – w, 78.67.Bf, 68.65. – k

### 1. INTRODUCTION

The II-VI chalcogenide nano-materials have a wide range of applications in variety of extends. Among them, cadmium sulfide (CdS), due to its considerable optical and electronic properties, has been using remarkably in the field of optoelectronics. The direct, wide energy band gap of CdS (about 2.4 eV. for bulk material) makes it a good candidate for using as a window layer in the second generation of solar cells [1, 2].

Small nanoparticles (diameter less than 10 nm) which also known as quantum dots (QDs) show the quantum confinement effects. One of the most important of those effects is the variation of band gap with the size of the particle. It has been found that when the size of nanoparticles are comparable or smaller than their exciton Bohr radius (5.8 nm for CdS), the band gap increases with decreasing particle size [3]. Size control and band gap tailoring makes QD nanoparticles very appropriate for different applications. In recent years CdS quantum dots (QDs) fabricated by SILAR (successive ionic layer adsorption and reaction) method on TiO<sub>2</sub> [4] or ZnO [5] photoanodes are widely used in quantum dot sensitized solar cells (QDSSCs). In addition CdS-QDs have been employed in the light emitting diodes [6, 7] and field-emission devices [8].

Since the nanoparticles are thermodynamically unstable, an agglomeration effect and as a consequent crystal growth can take place. To control the size of nanoparticles they are stabilized with organic systems that “enveloped them” and obstruct their agglomeration. Some polymers, organics or compounds have been utilized for this purpose as capping agents, like polyvinyl alcohol (PVA) [9], thiophenol [10], sodium citrate [11] and Sodium Hydroxide [12].

Various methods have been adopted for the synthesis of CdS nanocrystals including chemical bath deposition (CBD) [13, 14], Microwave assisted [15], chemical

precipitation technique [16], sol-gel [17] and successive ionic layer adsorption and reaction (SILAR) [18-21]. Also there are some reports on PVA capped CdS nanostructures (CdS/PVA nanocomposite) by CBD [22-26]. A complete and Comprehensive review on SILAR method is published by S.M. Pawar et al. [27]. For preparation of CdS nanostructures, the soda-lime glass is usually used as the substrate. On the other hand, Saglam et al. [28] synthesized CdS nanocrystals directly on the n-type Si substrates. Azizian et al. [29] used photographic gelatin film as a polymeric matrix.

Using a polymer matrix decreases the number of SILAR cycles, as reported that from about 50 cycles the nanoparticles were formed and poor crystallinity can be found [30]. For this purpose and because of its high dielectric constant (~ 28) [31], PVA is selected as a matrix to grow CdS quantum dots in this work. In addition, PVA matrix surface works as a seed medium and nucleation centers, for the growth of nanoparticles. Therefore, it controls the size and agglomeration of nanoparticles.

### 2. MATERIAL AND METHODS

All chemicals were used as received without any further purification. First of all, a 2% solution of PVA (MW = 72000 g/mol, from merck) in Double distilled water was prepared. After complete dissolution of polymer in the water, a series of PVA films were deposited on well cleaned soda-lime glasses with drop cast method. The PVA films left at room temperature for two days to dry completely. Aqueous solutions of 0.1 M/L Cadmium acetate ((CH<sub>3</sub>COO)<sub>2</sub>Cd × 2H<sub>2</sub>O from merck) and 0.1 M/L Sodium sulphide (Na<sub>2</sub>S × 9H<sub>2</sub>O from ACS) were used as cationic and anionic precursors, respectively. A SILAR cycle is carried out by immersing the substrate into the cationic precursor solution for 30 S, followed by washing the substrate with DI-water, and then immersing it into the anionic solution for 30 S, the

\* [n.memarian@semnan.ac.ir](mailto:n.memarian@semnan.ac.ir)

final step is again the washing step. This is one complete SILAR cycle. Washing step is done to prevent homogenous precipitation. Just after the first cycle, the light yellow color of the samples revealed that CdS nanostructures have been formed in the polymer matrix. This procedure has done up to 4 cycles.

UV-Vis absorption spectra were recorded on a Perkin Elmer Lambda 25, using a PVA film as a reference sample. The crystalline structure of the samples was investigated by X-ray diffraction (XRD) analysis with Bruker D8 Advance P.W. 3810 instrument, using Cu-K<sub>α</sub> radiation as the source. Atomic force microscopy (AFM) images of the samples surface were carried out by CP Research from Veeco Instruments Inc.

### 3. RESULTS AND DISCUSSION

#### 3.1 Optical Properties

Fig. 1 shows the optical absorbance spectra of the CdS/PVA samples with different cycles. The blue shift of absorption edge, due to small nanoparticle size, is clear. The value of the optical band gap energy ( $E_g$ ) can be determined from the absorption spectra by using Tauc's relation [32].

$$\alpha h\nu = B (h\nu - E_g)^n, \quad (3.1)$$

where  $h$  is the Planck's constant,  $B$  is a constant depending on the electron/ hole effective masses and  $n$  is a constant which depends on the nature of the transition between the valance band and conduction band. For direct transitions  $n = 1/2$  and for indirect transitions  $n = 2$ . The plot of  $(\alpha h\nu)^2$  versus  $h\nu$  for CdS nanoparticles with different cycles is shown in Fig. 2.

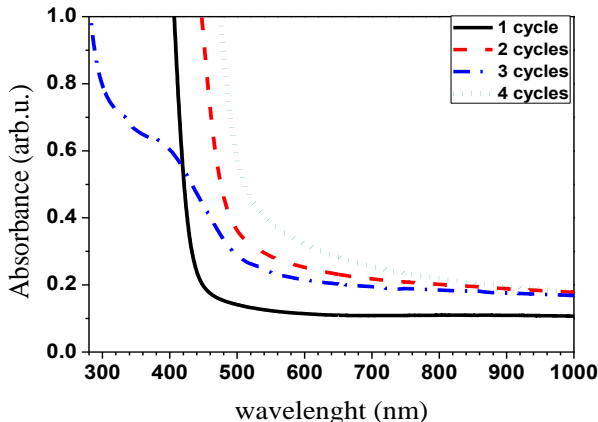


**Fig. 1** – Optical absorbance spectra of CdS nanoparticles with different SILAR cycles

By extrapolating the linear portion of the plots in Fig. 2 to the energy axis, the optical band gap values

**Table 1** – Description of the special paragraph styles

sample	$E_g$ (eV)	$R$ (EMA) (nm)	$D$ (XRD) (nm)	Interplanar distance (Å)
1 cycle	2.88	3.2	-	-
2 cycles	2.56	5.5	5.53	3.317
3 cycles	2.54	5.9	6.90	3.324
4 cycles	2.41	-	7.92	3.310

have been estimated. Band gap values for the samples are listed in Table 1. It is clear that by increasing the number of SILAR cycles the band gap is getting smaller and become closer to the bulk value.

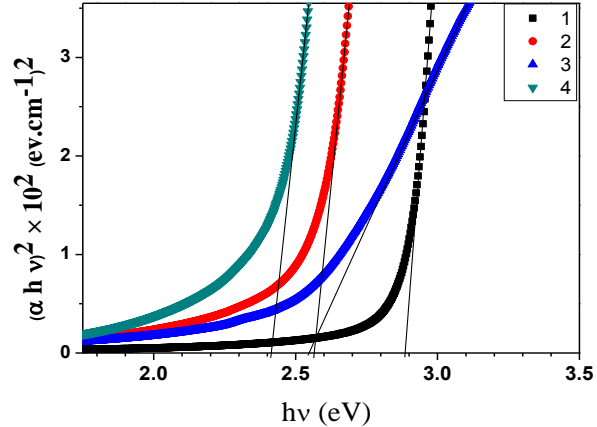


**Fig. 2** – Pplot of  $(\alpha h\nu)^2$  versus  $h\nu$  for CdS nanoparticles formed in PVA matrix with different cycles

The size of CdS nanoparticles is estimated through UV-Vis spectrophotometry, by comparison of the  $E_g$  values with a theoretical model. The Brus model [33, 34] is a theoretical model based on quantum mechanics known as the effective mass approximation (EMA). This model expresses a relationship between the  $E_g$  energy and the nanoparticle radius ( $r$ ) described by the equation (3.2):

$$E_{np} = E_g + \frac{\hbar^2 \pi^2}{2r^2} \left( \frac{1}{m_e^*} + \frac{1}{m_h^*} \right) - \frac{1.8e^2}{4\pi\epsilon_0\epsilon_r r}, \quad (3.2)$$

where  $E_{np}$  is the band gap energy of the CdS nanoparticle,  $E_g$  is the band gap energy of bulk CdS,  $e$  is the electron charge,  $r$  is the average nanoparticles size,  $m_e^*$  is the effective mass of electron (0.19  $m_e$  in CdS),  $m_h^*$  is the effective mass of hole (0.8  $m_e$  in CdS) [35],  $\epsilon_r$  is the high-frequency dielectric constant and  $\epsilon_0$  is the permittivity of vacuum. The second term in equation (3.2) referred to as the quantum localization term (like a particle in a box, for the exciton), which shifts the band gap to higher energies proportionally to  $r^{-2}$ . The third term in equation (3.2) arises due to the screened coulomb interaction between the electron and hole, it shifts  $E_{np}$  the to lower energy by a factor of  $r^{-1}$ . This term can be neglected due to high permittivity of the material. The calculated particle sizes were listed in Table 1.

The calculated average particle sizes using equation (3.2) are 3.2 nm, 5.5 nm and 5.9 nm for 1, 2 and 3 SILAR cycles, respectively. The size of nanoparticles for sample 1 to 3 is smaller than exciton Bohr radius. But

for sample with 4 SILAR cycles the band gap value is almost the same as bulk band gap value, so the EMA theory is not valid anymore.

### 3.2 Structural Analysis

Fig. 3 shows the X-ray diffraction (XRD) patterns of the samples. The sample which is labeled as PVA is the XRD pattern of a PVA film on glass substrate before fabrication of CdS-QDs. This sample is amorphous and shows no preferential orientation peak. The broad hump in that sample is due to amorphous glass substrate. As can be seen the sample with one SILAR cycle is also amorphous, this may be due to very small size of nanoparticles, so the Bragg reflections are poor and XRD cannot detect them, or because the entire polymer surface is not covered by CdS-QDs. By increasing the number of cycles, a broad peak can be seen at  $2\theta = 26.5^\circ$  which is related to the reflection from (111) plane of cubic CdS accordant with JCPD card No. 01-080-0019 with standard interplanar distance  $d = 3.355 \text{ \AA}$ . The intensity of this peak increases with increasing the number of cycles. The XRD patterns of samples 3 and 4 also exhibit another feeble, broad peak at  $2\theta = 43.9^\circ$  related to (220) plane. The XRD peaks are found to be very broad, indicating very fine size of the crystallites of the samples. It has been reported that the crystal phase of CdS depends on the crystallite size. Smaller CdS crystallites tend to show cubic lattice structure whereas larger crystallites normally have hexagonal structure [3].

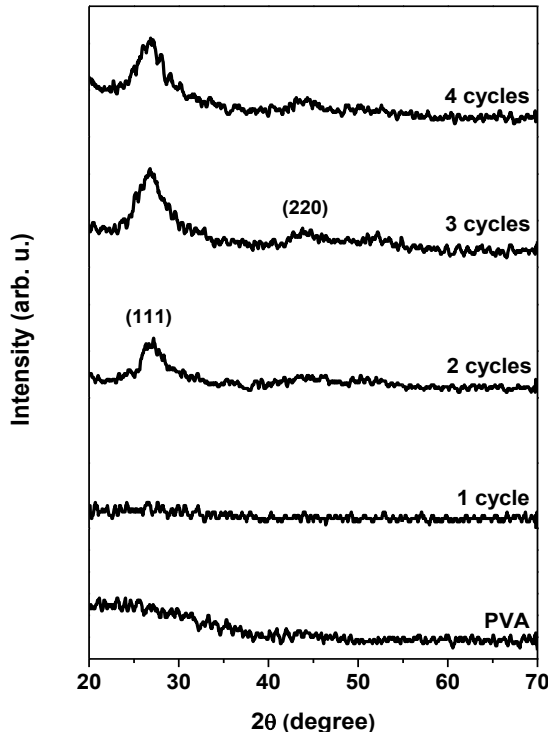


**Fig. 3 – XRD patterns of CdS/PVA samples with different cycles**

One of the most basic tasks in nanoscience is the accurate determination of particle sizes. Various methods have been developed to find out the mean particle diameter of nanocrystals. A very simple way to estimate the particle size from XRD data is its calculation from the

width of the Bragg reflections according to the Debye-Scherrer formula (equation (3.3)) [36]:

$$D_{D.S} = \frac{k \lambda}{\beta \cos \theta}, \quad (3.3)$$

where  $k$  is a constant related to the crystalline geometrical shape which is taken 0.9,  $\lambda$  is the wavelength of used X-ray (1.54 Å),  $\beta$  is the full width at half maximum (FWHM) and  $\theta$  is the diffraction angle. The applicability of the simple Scherrer formula for size determination from the XRD reflections is checked by Borchert et al. [37]. Calculation of the particle size with the Scherrer equation will lead to an effective diameter, which is smaller than the geometric diameter. For broad peaks it is better to refine and correct the Scherrer formula. In the case of spherical particles the corrections led to [37]:

$$D = \frac{4}{3} \frac{0.9 \lambda}{\beta \cos \theta}, \quad (3.4)$$

Structural parameters such as crystallite size and interplanar distance are listed in Table 1. The values of crystallite size calculated from XRD analysis are in great agreement with those estimated from EMA theory. The decrease in interplanar distances compared to the standard value could be due to the fine size of crystallites. The style, which is used to format the headers and footers.

### 3.3 AFM Morphology

To find out detailed morphological properties of the samples surface, atomic force microscopy (AFM) is employed. AFM is also an appropriate method for investigation and quantitative measurement of surface roughness parameters. Some important roughness parameters are  $R_q$ : root mean squared (RMS) roughness,  $R_a$ : average roughness,  $R_p$ : maximum peak height,  $R_v$ : maximum valley depth. These parameters are listed in Table 2. Two dimensional (2D) and three dimensional (3D) pictures of the samples surface are shown in Fig. 4 to 6.

In Fig. 4 the surface of PVA sample, before fabrication of nanoparticles, is shown. This surface is very smooth without any texture or agglomeration of particles. For more precision the scale of this sample is smaller than other samples. It is also clear from Table 2 that this surface is very smooth and all roughness parameters are small. From Fig. 5 one can see that after the first cycle there is a steep increase in all roughness parameters, especially in  $R_q$  and  $R_a$  which shows the growth of nanostructures on the PVA surface.

**Table 2 – Roughness data and average grain sizes of the samples from AFM analysis**

Sample	$R_q$ (nm)	$R_a$ (nm)	$R_p$ (nm)	$R_v$ (nm)	Average grain size (nm)
PVA	2.25	1.51	13.49	-26.67	-
1 cycle	30.78	24.48	64.30	-68.76	190.0
2 cycles	19.57	16.31	43.84	-43.44	214.8
3 cycles	27.63	19.86	78.58	-114.8	302.7
4 cycles	148.6	115.9	255.7	-324.2	1320.0

The separated spherical agglomerations can be detected with a size about 190 nm. It can be said that the entire surface has not been covered at the first cycle. The AFM image of the sample with two SILAR cycles is shown in Fig. 6. It is clear that the agglomerations of nanoparticles are grown. At the first glance this is in contrary with data in Table 2, since the roughness parameters are lower than data for the sample with 1 cycle. This may be due to saturation and complete coverage of the surface

by nanoparticles. Because of that the surface is smoother than the 1cycle. After this stage, the clusters are getting larger and augment the size. From the third cycle, by increasing the number of SILAR cycle the roughness of the surface increases. The AFM image of the sample with 3 SILAR cycles. Entire the surface is covered by CdS nanoparticles. Finally, for the 4 cycles the clusters are growth and gross grains have been formed.

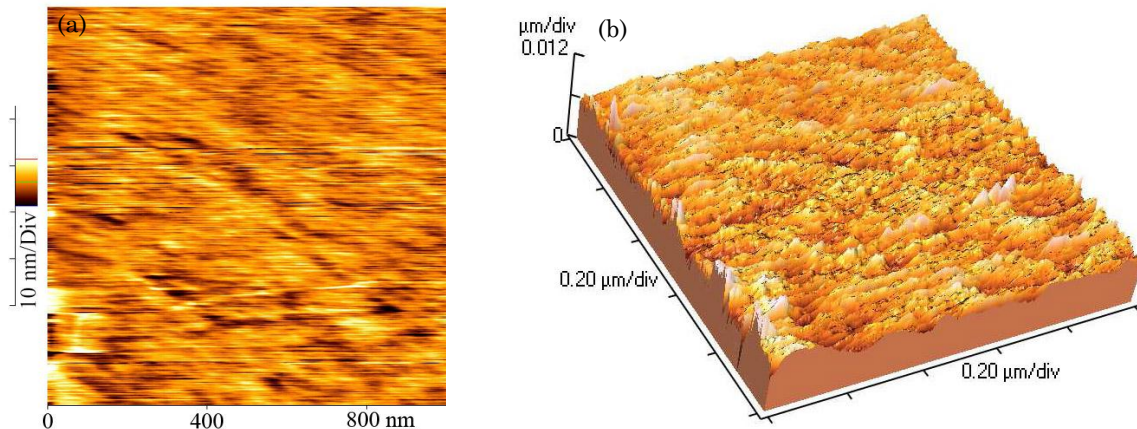


**Fig. 4 – 2D (a) and 3D AFM micrograph of a PVA film surface (b)**

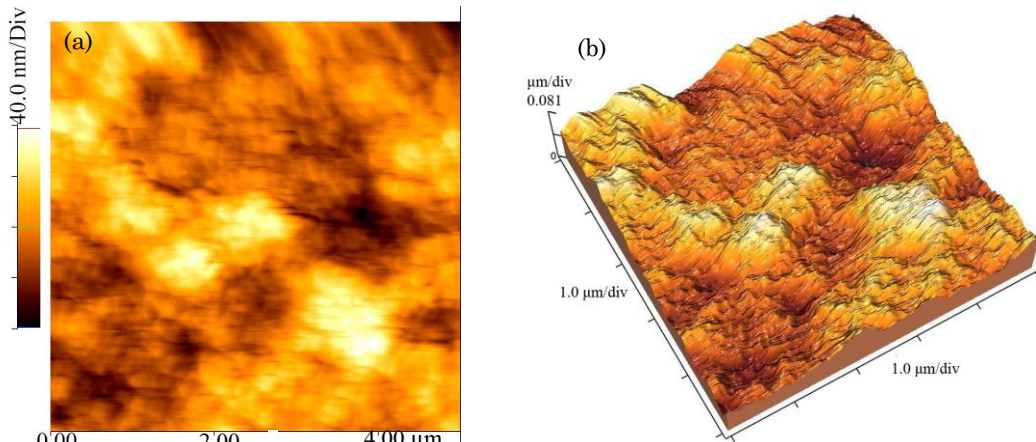


**Fig. 5 – 2D (a) and 3D AFM image of CdS nanostructures after 1 SILAR cycles (b)**

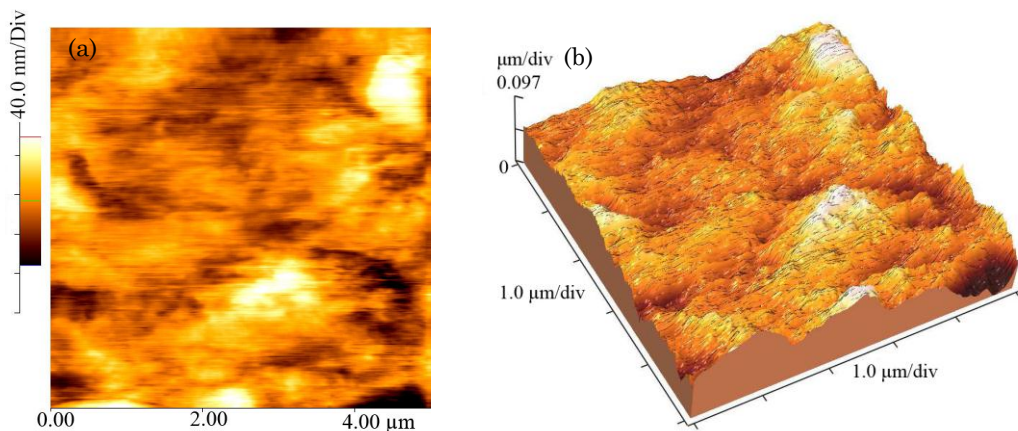


**Fig. 6 – 2D (a) and 3D AFM image of CdS nanostructures after 2 SILAR cycles (b)**

#### 4. CONCLUSIONS

CdS nanoparticles have been grown on the PVA matrix surface on glass substrates, by SILAR method. With fewer cycles we have found that CdS quantum dots have been fabricated. XRD analysis of these small crystallites showed that just after the second cycle, cubic crystal structure with (111) preferred orientation is formed. Particle sizes are estimated from the band gap values using the EMA theory. Those are in good

agreement with XRD results. From optical investigations, direct band gap of the samples was found between 2.88 and 2.41 eV. Studies on morphology of the surface showed the agglomeration of nanocrystallites. By increasing the number of SILAR cycle the roughness of the surface increased. Simple and facile route, low number of cycles and tunable band gap make this method very efficient to make quantum dots for different applications such as QDSSCs, OLEDs and other optoelectronic devices.

#### REFERENCES

1. W.F. Mohammed, O. Daoud, M. Al-Tikriti, *Circuit. Syst.* **3**, 230 (2012).
2. I.M. Dharmadasa, P.A. Bingham, O.K. Echendu, H.I. Salim, T. Druffel, R. Dharmadasa, G.U. Sumanasekera, R.R. Dharmasena, M.B. Dergacheva, K.A. Mit, K.A. Urazov, L. Bowen, M. Walls, A. Abbas, *Coatings* **4**, 380 (2014).
3. R. Ahmed, G. Will, J. Bell, H. Wang, *J. Nanopart. Res.* **14**, 1140 (2012).
4. I. Concina, N. Memarian, G.S. Selopal, M.M. Natile, G. Sberveglieri, A. Vomiero, *J. Power Sources* **240**, 736 (2013).
5. M. Thambidurai, N. Muthukumarasamy, N. Sabari Arul, S. Agilan, R. Balasundaraprabhu, *J. Nanopart. Res.* **13**, 3267 (2011).
6. X. Dai, Z. Zhang, Y. Jin, Y. Niu, H. Cao, X. Liang, L. Chen, J. Wang, X. Peng, *Nature* **515**, 96 (2014).
7. J. Zhao, J.A. Bardecker, A.M. Munro, M.S. Li, Y. Niu, I.K. Ding, J. Luo, B. Chen, A.K.Y. Jen, D.S. Ginger, *Nano Lett.* **6**, 463 (2006).
8. P.K. Ghosh, S. Jana, U.N. Maity, K.K. Chattopadhyay, *Physica E* **35**, 178 (2006).
9. H. Wang, P. Fang, Z. Chen, and S. Wang, *Appl. Surf. Sci.* **253**, (2007) 8495.
10. M. Pattabi, B.S. Amma, *Sol. Energy Mater. Sol. Cells* **90**, 2377 (2006).
11. D. Philip, *Physica E* **41**, 1727 (2009).
12. R. Sakthivishnu, R. Nithya, M. Alagappan, N. Meenakshi Sundaram, *J. NanoSci. NanoTech.* **2**, 90 (2014).
13. Suresh Kumar, Santosh Kumar, P. Sharma, V. Sharma, S.C. Katyal, *J. Appl. Phys.* **112**, 123512 (2012).
14. R. Demir, F. Gode, *Chalcogen. Lett.* **12**, 43 (2015).
15. I. A. Lopez, A. Vazquez, I. Gomez, *Rev. Mex. Fis.* **59**, 160 (2013).
16. R.R. Prabhu, M. Abdul Khadar, *Pramana J. Phys.* **65**, 801 (2005).
17. S.M. Reda, *Acta Mater.* **56**, 259 (2008).
18. S. Patra, P. Mitra, S.K. Praghan, *Mater. Research* **14**, 17 (2011).
19. K. Manikandan, P. Mani, P.F.H. Inbaraj, T.D. Joseph, V. Thangaraj, C.S. Dilip, J.J. Prince, *Indian J. Pure Appl. Phys.*, **52**, 354 (2014).
20. B.R. Sankpal, R.S. Mane, C.D. Lokhande, *Mater. Research Bull.* **35**, 177 (2000).
21. C.D. Lokhande, B.R. Sankpal, H.M. Pathan, M. Muller, M. Giersig, H. Tributsch, *Appl. Surf. Sci.* **181**, 277 (2001).
22. L. Sujata Devi, K. Nomita Devi, B. Indrajit Sharma, H. Nandakumar Sarma, *Chalcogenide Lett.* **9**, 67 (2012).
23. D. Saikia, P.K. Saikia, P.K. Gogoi, M.R. Das, P. Sengupta, M.V. Shelke, *Mater. Chem. Phys.* **131**, 223 (2011).
24. J.C. Ferrer, A. Salinas-Castillo, J. L. Alonso, S. Fernandez de Avila, R. Mallavia, *Mater. Lett.* **63**, 638 (2009).
25. R. Devi, P. Purkayastha, P.K. Kalita, B.K. Sarma, *Bull. Mater. Sci.* **30**, 123 (2007).
26. P.K. Khanna, R.R. Gokhale, V.V.V.S. Subbarao, N. Singh, K.W. Jan, B.K. Das, *Mater. Chem. Phys.* **94**, 454 (2005).
27. S.M. Pawar, B.S. Pawar, J.H. Kim, Oh-Shim Joo, C.D. Lokhande, *Curr. Appl. Phys.* **11**, 117 (2011).
28. M. Saglam, A. Ates, B. Guzeldir, M.A. Yildirim, A. Astam, *Microelectron. Eng.* **85**, 1831 (2008).
29. Y. Azizian, M. Muradova, R. Mammedova, A. Khodayari, *J. Cryst. Growth*, **305**, 175 (2007).
30. K.G. Rao, V.K. Ashith, *J. Phys. Chem. Solids* **77**, 14 (2015).
31. S. Jana, R. Thapa, R. Maity, K.K. Chattopadhyay, *Physica E* **40**, 3121 (2008).
32. B.D. Viezbicke, Sh. Patel, B.E. Davis, D.P. Birnie, *Phys. Status Solidi B* **252**, 1700 (2015).
33. S. Baset, H. Akbri, H. Zeynali, M. SHafie, *Digest J. Nanomat. Biostr.* **6**, 709 (2011).
34. O.E. Chukwuocha, M.C. Onyeaju, T.S.T. Harry, *World J. Cond. Matt. Phys.* **2**, 96 (2012).
35. D.S. Yoo, S.Y. Ha, I.G. Kim, M.S. Choo, K.W. Kim, E.S. Lee, *New Physics: Sae Mulli* **61**, 680 (2011).
36. N. Memarian, S.M. Rozati, E. Elamurugu, E. Fortunato, *Phys. Status Solidi C* **7**, 2277 (2010).
37. H. Borchert, E.V. Shevchenko, A. Robert, I. Mekis, A. Kornowski, G. Grubel, H. Weller, *Langmuir* **21**, 1931 (2005).